Progress In Electromagnetics Research C, Vol. 120, 209–222, 2022

Design and Analysis of Multiband Fractal Reconfigurable Antenna Using PIN Diodes for Smart Wireless Communications

Iqra Masroor*, Jamshed A. Ansari, Amrees Pandey, and Piyush K. Mishra

Abstract—Fractal and reconfigurable antennas are the need of modern wireless communication systems that operate under dynamic scenarios catering to the diversified needs of modern wireless applications. In this dissemination, a novel multiband Fractal Reconfigurable Antenna (FRA) is presented and discussed using two RF PIN diodes as switching elements for electronic reconfiguration. It is analyzed using equivalent circuit concept and investigated in terms of various antenna performance parameters. The proposed FRA can operate in various frequency bands resonating at four different frequencies with switchable bandwidth and gain. The highest gain is observed to be about 8.37 dB at 9.68 GHz while the highest bandwidth is about 540 MHz in the X-band. The simulation and measurement results obtained are found in agreement. The multiband characteristics of the proposed FRA make it useful for smart wireless communication applications in the S (2–4 GHz), C (4–8 GHz), and X (8–12 GHz) microwave bands.

1. INTRODUCTION

Microstrip patch antennas have undergone numerous modifications in their basic configuration to cater to the growing need of wireless communication technology. Besides being in great demand because of their attractive features, their ease of integration with current advances in design approaches has further improved their performance. The use of different feed techniques, substrate materials, parasitic patches, patches with slots/notches, defected ground structures, fractal geometries, electronic reconfiguration, and a lot more has been explored in order to achieve better antenna performance parameters. Fig. 1 depicts the various design approaches that have been explored for enhanced antenna performance and how they have led to the evolution of microstrip patch antenna over the years.

Unique properties exhibited by a class of geometry known as fractals have enabled antenna designers to achieve antenna miniaturization [1]. Fractals, being self-similar and composed of many scaled replicas of themselves, have been hugely exploited by researchers to create novel antenna designs that have multiband characteristics and compactness in size [2]. The use of fractal geometry in [3] provides an increase in the electrical length of the patch without having to actually increase the patch area, thus, providing compactness in antenna size. An interesting octagonal fractal microstrip patch antenna has been reported in [4] having super wideband characteristics.

Reconfiguration of patch antenna can also be achieved using various switching elements such as PIN diodes and varactor diodes in order to attain polarization, frequency or radiation pattern reconfigurability. Frequency reconfigurable antennas capable of operating in various frequency bands have been extensively reported in literature [5–8]. Polarization reconfigurability, such as the ability to switch polarization states between linear and circular polarizations, Right Hand Circular Polarization (RHCP), and/or Left Hand Circular Polarization (LHCP), can be attained by appropriate mounting and biasing of the PIN diode switches in the basic antenna geometry [9–11]. Another class of antenna

Received 14 April 2022, Accepted 19 May 2022, Scheduled 4 June 2022
* Corresponding author: Iqra Masroor (iqraec1029@gmail.com).
The authors are with the Department of Electronics and Communication, University of Allahabad, Prayagraj, India.

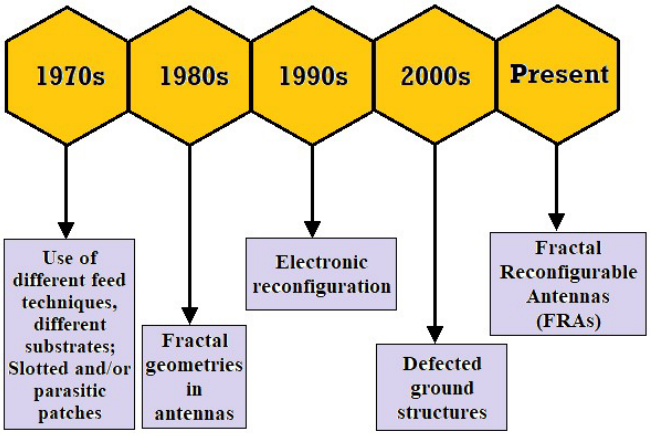

Figure 1. Evolution of Microstrip Patch Antenna (MPA) using various design approaches over the years.

reconfigurability is reconfigurable radiation patterns. The ability to reconfigure the radiation pattern characteristics can improve the whole system performance of antenna [12]. A dual-reconfigurable antenna providing both frequency and pattern reconfigurability has been proposed in [13].

Combining fractal geometries with reconfigurability can lead to multifunctional antenna designs which are the need of current and future wireless communication applications. Such fractal and reconfigurable microstrip patch antennas have been recently explored for enhanced antenna performance [14–17]. In this work, a multiband Fractal Reconfigurable Antenna (FRA) has been analyzed and designed by making use of two PIN diodes as switching components. The simulation and measurement results have been investigated and discussed.

2. DEVELOPMENT AND DESIGN OF PROPOSED FRA

In this section, the development of proposed FRA design has been discussed, followed by theoretical considerations and equivalent circuit and the resulting geometry of the proposed design.

2.1. Design of Rectangular Microstrip Patch Antenna (RMPA)

The development of the proposed antenna starts with the design of a fundamental Rectangular Microstrip Patch Antenna (RMPA) at a design frequency of 3.8 GHz. Fig. 2 shows the schematic of RMPA. The substrate material used is low-cost FR4-epoxy of thickness (h) 1.6 mm, relative permittivity (ε_r) 4.4, and dielectric loss tangent (δ) 0.02. A simple microstrip line feed has been used to provide

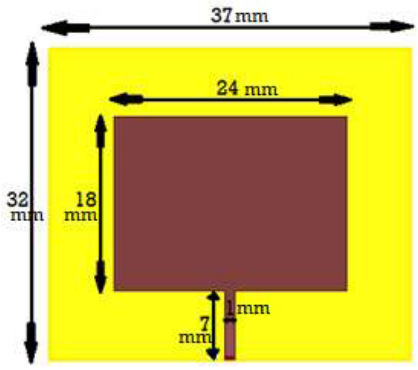

Figure 2. Schematic of Rectangular Microstrip Patch Antenna (RMPA).

excitation to the radiating patch such that proper impedance matching is obtained. Using the below mathematical equations, the patch dimensions of the RMPA have been determined [18, 19].

The length of the rectangular patch is given by:

$$l_{patch} = l_e - 2\Delta L \tag{1}$$

where l_e is the effective length of the patch, given by:

$$l_e = \frac{c}{2f_r\sqrt{\varepsilon}_e} \tag{2}$$

where c is the velocity of light, f_r the design/resonant frequency, and ε_e the effective permittivity of substrate, given by:

$$\varepsilon_e = \frac{\varepsilon_r + 1}{2} + \frac{\varepsilon_r - 1}{2}\left[1 + \frac{12h}{w_{patch}}\right]^{-\frac{1}{2}} \tag{3}$$

where ε_r is the relative permittivity of the substrate.

The fringing length (ΔL) is determined using:

$$\frac{\Delta L}{h} = 0.412\frac{(\varepsilon_e + 0.3)\left(\frac{w_{patch}}{h} + 0.264\right)}{(\varepsilon_e - 0.258)\left(\frac{w_{patch}}{h} + 0.8\right)} \tag{4}$$

where h is the substrate thickness, and w_{patch} is the width of the rectangular patch, given by:

$$w_{patch} = \frac{c}{2f_r\sqrt{\frac{\varepsilon_{r+1}}{2}}} \tag{5}$$

For the design frequency (f_r) of 3.8 GHz, the patch dimensions obtained are 18 mm × 24 mm, and the ground dimensions are kept to 32 mm × 37 mm, so as to make the RMPA resonate at or near about the intended design frequency.

2.2. Inclusion of Fractal Slots on Antenna Patch

In order to utilize the beauty of fractals to achieve size compactness and multiband characteristics, the antenna is fractaled using triangular slots on the radiating patch as shown in Fig. 3. The first iteration consists of two equilateral triangular slots having side dimension of $3\sqrt{3}$ mm etched on the left and right sides of the patch with the horizontal axis of the triangles lying in the center of the patch. The second iteration is obtained from the first iteration by etching two more equilateral triangular slots on either side with a scaled-down side dimension of $1.5\sqrt{3}$ mm. The third iteration is obtained from the second iteration by further etching two more equilateral triangular slots on either side with side-dimension further scaled down to $0.75\sqrt{3}$ mm; the scaling factor for each fractal iteration is 1/2. In every iteration, the start position (vertex) of the previous iteration slot becomes the center position (centroid) of the next iteration slot as shown in Fig. 3. This leads to the formation of slot loaded patch consisting of slots S_1 and S_2 such that slot S_1 is composed of slots S_{11}, S_{12}, and S_{13}, and slot S_2 is composed of slots S_{21}, S_{22}, and S_{23}.

2.3. Use of PIN Diodes as Switching Elements and Resulting FRA Geometry

A rectangular notch, named N, having dimension of 16.65 mm × 1.8 mm, is loaded onto the patch so as to aid the placement of PIN diodes. In the third iteration fractal patch antenna, two PIN diodes, one at the top of the notch, named D_1, and the other in the middle of the notch, named D_2, have been included to make the proposed antenna reconfigurable as shown in Fig. 4. Lumped RLC model of PIN diode has been constructed using parameters from the technical datasheet of the diode NXP BAP50-03 [20]. The width of the slot has been taken as 1.8 mm considering the dimension of the PIN diode used (1.35 mm × 1.8 mm). In the ON-state, the diodes are assumed to behave as a short circuit having an inductance ($L = 1.8$ nH) in series with the ON-state resistance ($R_{on} = 5\,\Omega$), and in the OFF-state, the diodes are assumed to behave as an open-circuit having the inductance ($L = 1.8$ nH) in series

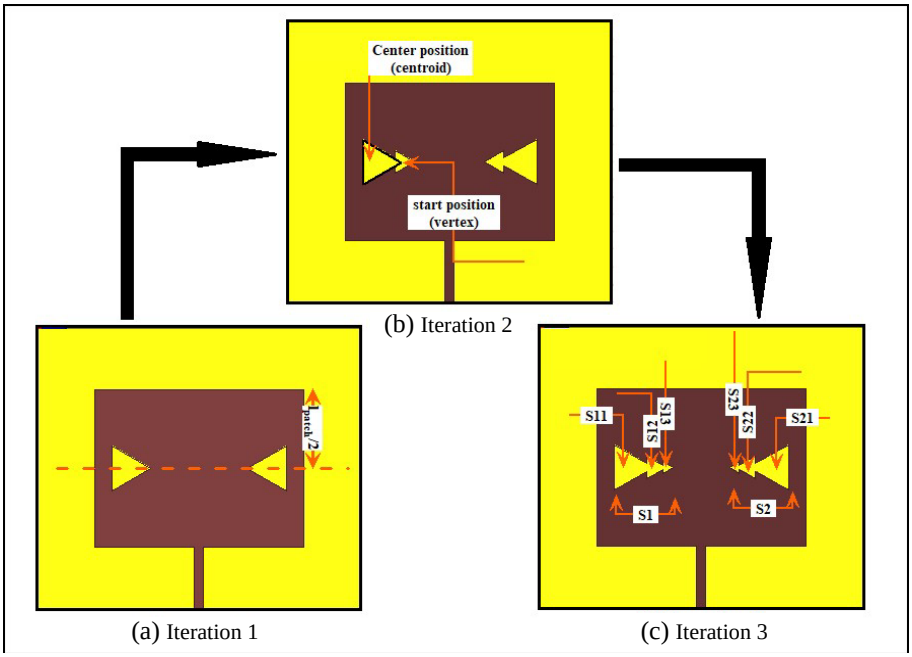

Figure 3. Fractal slots on antenna patch.

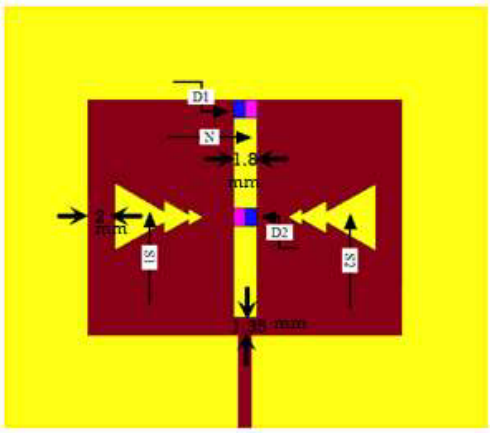

Figure 4. Final geometry of proposed FRA.

with a parallel combination of the OFF-state resistance $R_{off} = 500\,\text{k}\Omega$ and capacitance ($C = 0.35\,\text{pF}$) [11]. The lumped RLC model of PIN diode and its RLC equivalent circuit are as shown in Fig. 5(a) and Fig. 5(b), respectively. It is noted that the two diodes conduct current in opposite directions when being switched ON. The direction of current flow through the diodes is as depicted in Fig. 5(a).

2.4. Equivalent Circuit Analysis and Theoretical Considerations

The equivalent circuit of a conventional rectangular microstrip patch is considered to be a parallel combination of resistance (R_P), inductance (L_P), and capacitance (C_P), as shown in Fig. 6(a). The total input impedance (Z_P) of the microstrip patch is, therefore, given by [19]:

$$Z_P = \frac{1}{\dfrac{1}{R_P} + j\omega C_P + \dfrac{1}{j\omega L_P}} \tag{6}$$

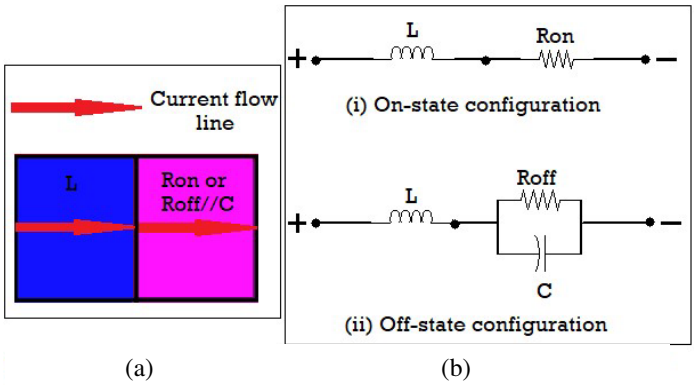

Figure 5. (a) Lumped RLC model of PIN diode, (b) RLC equivalent circuit of diode [(i) On-state configuration, (ii) Off-state configuration].

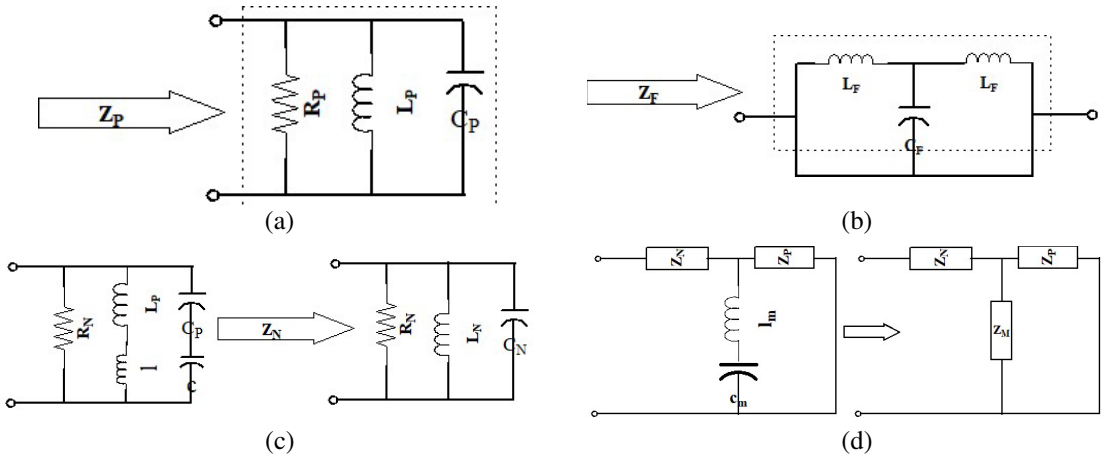

Figure 6. (a) Equivalent circuit of rectangular patch, (b) equivalent circuit of microstrip feed line, (c) equivalent circuit due to the effect of notch (N), (d) equivalent circuit of coupled notch loaded rectangular patch.

The circuit parameters are given as [19]:

Capacitance,

$$C_P = \frac{\varepsilon_e \varepsilon_o l_{patch} w_{patch}}{2h} \cos^{-2}\left(\frac{\pi x_o}{l_{patch}}\right) \tag{7}$$

Inductance,

$$L_P = \frac{1}{\omega^2 C_P} \tag{8}$$

Resistance,

$$R_P = \frac{Q_r}{\omega C_P} \tag{9}$$

where l_{patch} is the length, w_{patch} the width of the rectangular patch, h the substrate thickness, x_o the feed location along the length of the patch, ε_e the effective permittivity of the medium, and the total quality factor (Q_r) of the resonating circuit is given by:

$$Q_r = \frac{c\sqrt{\varepsilon}_e}{4 f_r h} \tag{10}$$

where f_r is the resonant frequency, and c is the velocity of light.

The equivalent circuit of the simple microstrip line-feed, connected at the edge of the radiating patch, as shown in Fig. 6(b), is considered to be a parallel combination of L_F and C_F, where L_F and C_F are the inductance and capacitance of the strip-feed, respectively [21].

Insertion of the rectangular notch (N), as shown in Fig. 4, results in the flow of two currents: the patch current which causes the antenna to resonate at the design frequency and an additional current that flows around the notch causing a second resonant frequency. To account for this modification, an additional series inductance (l) and series capacitance (c) are included in the equivalent circuit, modifying it, as shown in Fig. 6(c) [22, 23].

The input impedance (Z_N) of the notch loaded patch is given by [22, 23]:

$$Z_N = \frac{1}{\frac{1}{R_N} + j\omega C_N + \frac{1}{j\omega L_N}} \tag{11}$$

where R_N is the resistance due to the effect of the notch on patch and can be calculated in a similar manner as R_P while the notch capacitance (C_N) and notch inductance (L_N) are given by [18]:

$$C_N = \frac{c \cdot C_P}{c + C_P} \tag{12}$$

$$L_N = L_P + l \tag{13}$$

This results in two resonating circuits, one being the initial patch circuit and the other being the notch loaded patch circuit. The two resonant circuits are coupled through mutual inductance (l_m) and mutual capacitance (C_m), resulting in the modified patch circuit as shown in Fig. 6(d).

The slots, S_1 and S_2, as shown in Fig. 4, loaded on the patch are considered as parallel combinations of the impedances of the first iteration, second iteration, and third iteration slots, respectively. For the slots, input impedance (Z_{SLOT}) can be evaluated as [24, 25]:

$$Z_{SLOT} = R_{SLOT} + jX_{SLOT} \tag{14}$$

where R_{SLOT} and X_{SLOT} are the real and imaginary parts of the slot impedance respectively as shown in Fig. 7(a).

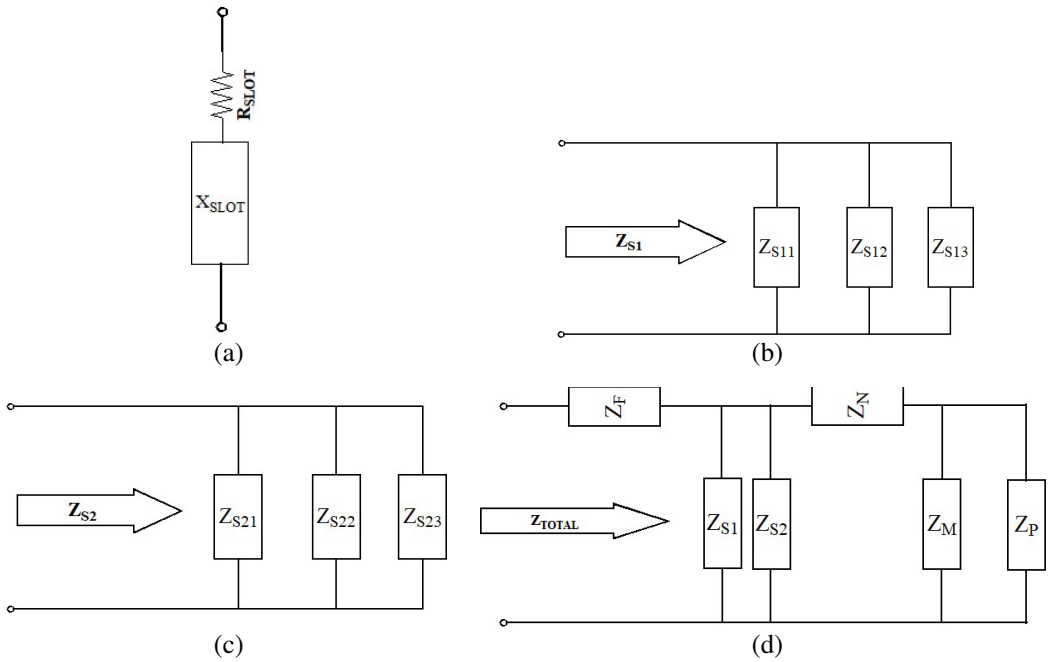

Figure 7. (a) Equivalent circuit of a slot, (b) equivalent circuit of slot S_1, (c) equivalent circuit of slot S_2, (d) resulting equivalent circuit of notch and slot loaded patch.

Input impedances, Z_{S_1} and Z_{S_2} for the slots S_1 and S_2, as shown in Fig. 7(b) and Fig. 7(c), respectively, are given by:

$$Z_{S_1} = \frac{1}{\frac{1}{Z_{S_{11}}} + \frac{1}{Z_{S_{12}}} + \frac{1}{Z_{S_{13}}}} \tag{15}$$

$$Z_{S_2} = \frac{1}{\frac{1}{Z_{S_{21}}} + \frac{1}{Z_{S_{22}}} + \frac{1}{Z_{23}}} \tag{16}$$

where $Z_{S_{11}}$, $Z_{S_{12}}$, and $Z_{S_{13}}$ are the input impedances of the first iteration, second iteration, and third iteration slots in the slot S_1, and $Z_{S_{21}}$, $Z_{S_{22}}$, and $Z_{S_{23}}$ are the input impedances of the first iteration, second iteration, and third iteration slots in slot S_2 [26, 27].

The resulting equivalent circuit of the notch and slot loaded patch is as depicted in Fig. 7(d). For the resulting circuit, the total input impedance (Z_{TOTAL}) can, therefore, be evaluated as:

$$Z_{TOTAL} = Z_F + \frac{\left(\frac{Z_{S_1} \cdot Z_{S_2}}{Z_{S_1} + Z_{S_2}}\right) \cdot \left(Z_N + \frac{Z_M \cdot Z_P}{Z_M + Z_P}\right)}{\left(\frac{Z_{S_1} \cdot Z_{S_2}}{Z_{S_1} + Z_{S_2}}\right) + Z_N + \left(\frac{Z_M \cdot Z_P}{Z_M + Z_P}\right)} \tag{17}$$

Using Z_{TOTAL}, the following antenna parameters can be easily determined, such as:

Reflection coefficient:

$$\Gamma = \frac{Z_{TOTAL} - Z_o}{Z_{TOTAL} + Z_o} \tag{18}$$

where Z_o is the input impedance of the microstrip-feed ($50\,\Omega$).

Voltage Standing Wave Ratio:

$$\text{VSWR} = \frac{1 + |\Gamma|}{1 - |\Gamma|} \tag{19}$$

Return Loss:

$$RL = 20\log|\Gamma| \tag{20}$$

3. DISCUSSION OF RESULTS

Finite element method solver Ansys HFSS simulation tool has been used to observe and investigate the results of the proposed design. The fabricated prototype of proposed FRA is as shown in Fig. 8. In this section, the effects of the inclusion of fractal slots and PIN diode switches have been examined, and results obtained from simulation and measurements have been discussed.

3.1. Effect of Fractal Iterations

Figure 9 shows the variation of return loss in dB with respect to frequency for various fractal iterations. It is observed that for the first iteration fractaled patch, the initial resonating frequency of the antenna is at 3.7 GHz; for the second iteration fractaled patch, the resonating frequency is lowered to 3.5 GHz while the return loss at other resonant frequencies is also improved; for the third iteration fractaled patch, the multiband characteristics are further enhanced with improved S_{11} parameters at the resonating frequencies. Lower resonating frequencies and multiband characteristics are, thus, obtained along with reduction in patch area as the number of iterations is increased up to the third iteration.

3.2. Near-Field and Far-Field Characteristics

Figure 10 demonstrates the experimental setup for measurement of the near-field characteristics of the proposed antenna using Vector Network Analyzer (VNA) from Agilent Technologies N5247A. The operating modes assigned for the four switching cases of the diodes, D_1 and D_2, with simulated and measured resonating frequencies and corresponding return losses, are as noted in Table 1. The effect

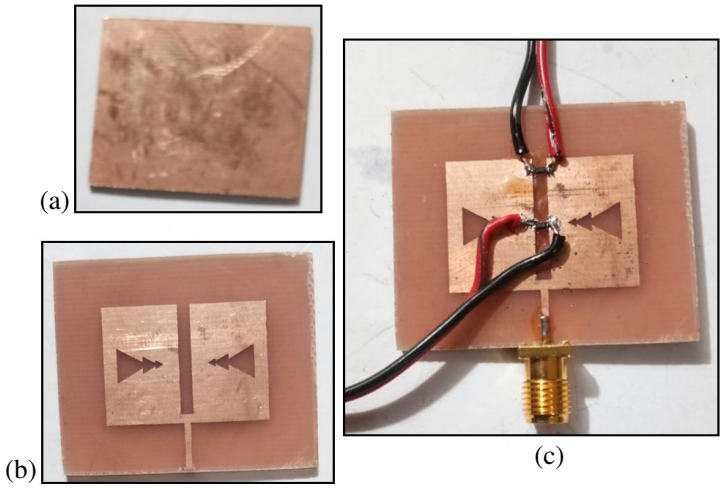

Figure 8. Fabricated antenna prototype, (a) bottom-view (ground), (b) top-view (patch), (c) proposed FRA with PIN diodes.

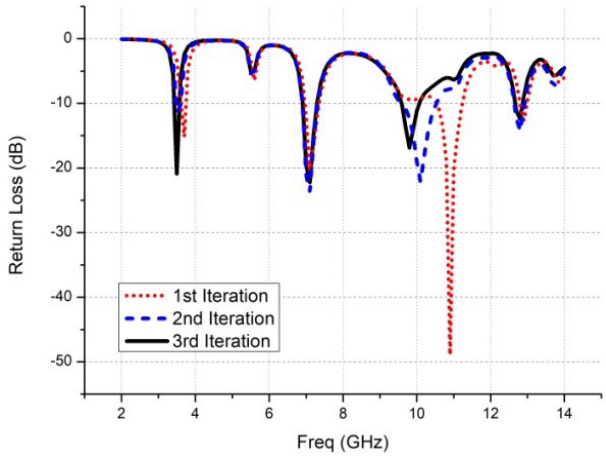

Figure 9. Variation of return loss with frequency for various fractal iterations.

of diode D_1 is demonstrated by the return loss plot, shown in Fig. 11, which shows the behaviour of proposed antenna under On and Off conditions of diode D_1. The variations of simulated and measured return losses of the proposed FRA with frequency for all the switching cases of diodes are as shown in Fig. 12. The simulated and measured return losses are observed to be in close agreement. The -10 dB simulated impedance bandwidth, observed to be 540 MHz, is the highest for mode: 1110 when both the diodes are in the ON state. The minimum and maximum values of the simulated peak gain for the proposed FRA are observed to be 3.36 dB and 8.37 dB for mode: 0101 and mode: 1110, respectively. It is noted that the bandwidth and gain can be adjusted as desired depending on the switching states of the diode. The variations of measured VSWR and measured antenna peak gain as a function of frequency are as illustrated in Fig. 13. Simulated values of VSWR, impedance bandwidth, and peak gain for all the operating modes are as noted in Table 2.

For the assessment of far-field radiation characteristics, the proposed FRA in an anechoic chamber setup is as shown in Fig. 14. The radiation patterns provide a graphical representation of the antenna radiation characteristics and are as illustrated in Fig. 15. Far-field radiation patterns of the proposed FRA are observed to be nearly omnidirectional, and the simulated and measured patterns agree more nearing higher resonant frequencies. Deviations exist between simulated and measured results owing to fabrication and measurement errors and sensitivity of the PIN diodes to electrical biasing.

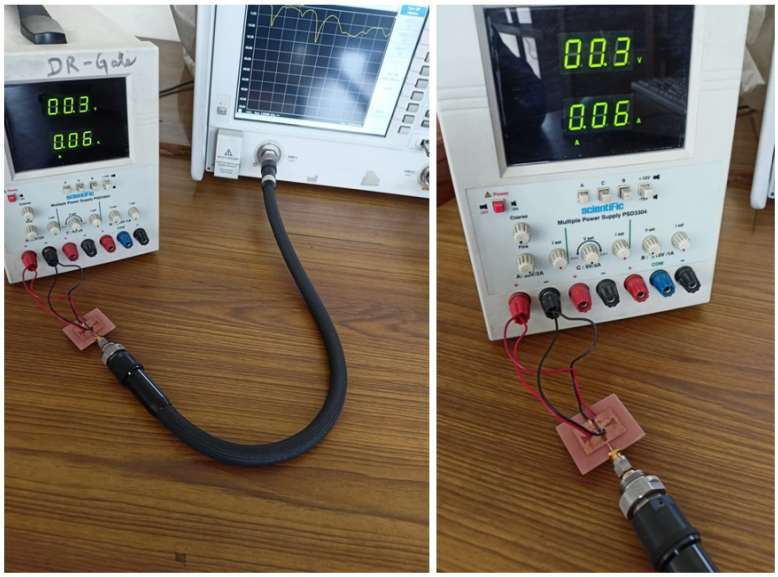

Figure 10. Measurement setup with VNA.

Table 1. Resonant frequencies and return loss for various operating modes.

Switching Cases	Modes	Resonant Frequencies (GHz)		Return Loss (dB)	
		SIM	MEAS	SIM	MEAS
D_1 OFF, D_2 OFF	0000	3.50	3.38	−12.91	−11.56
	0001	6.98	7.64	−15.08	−9.81
	0010	9.74	9.86	−17.65	−14.68
	0011	12.68	11.12	−17.70	−19.30
D_1 OFF, D_2 ON	0100	3.50	3.38	−17.79	−11.34
	0101	7.04	7.64	−17.62	−14.78
	0110	9.74	9.86	−16.17	−16.23
	0111	12.74	11.18	−15.26	−23.55
D_1 ON, D_2 OFF	1000	3.50	3.38	−18.73	−12.85
	1001	7.10	7.52	−23.07	−26.98
	1010	9.62	9.80	−22.60	−23.19
	1011	12.80	11.06	−11.45	−25.14
D_1 ON, D_2 ON	1100	3.44	3.38	−13.13	−7.65
	1101	6.92	7.64	−25.15	−21.22
	1110	9.68	9.86	−27.44	−27.52
	1111	12.44	11.06	−27.24	−22.04

3.3. Comparative Report

The proposed work has been compared with some existing designs reported in literature [14–17]. The comparison, as noted in Table 3, shows that the proposed design provides more number of reconfigurable operating microwave bands using only two RF switches with significant peak gain as opposed to other works that require more than two switches.

Table 2. VSWR, impedance bandwidth and peak gain for various operating modes.

Modes	VSWR	Impedance Bandwidth (MHz)	Peak gain (dB)
0000	1.58	100	3.84
0001	1.42	320	3.69
0010	1.30	480	8.16
0011	1.29	280	3.92
0100	1.29	110	3.88
0101	1.30	330	3.36
0110	1.36	480	7.49
0111	1.41	230	3.90
1000	1.26	100	3.87
1001	1.15	380	3.67
1010	1.16	510	6.87
1011	1.72	130	3.78
1100	1.56	70	3.76
1101	1.11	400	4.28
1110	1.08	540	8.37
1111	1.09	380	3.82

Table 3. Comparative report.

Reference	Year	Microwave Bands	No. of RF switches used	Peak gain (dB)
[14]	2019	S, C	Two	4.438
[15]	2014	S, C, X	Four	5.46
[16]	2016	S, C, X	Six	-
[17]	2019	S, C, X	Six	-
Proposed work	-	S, C, X	Two	8.37

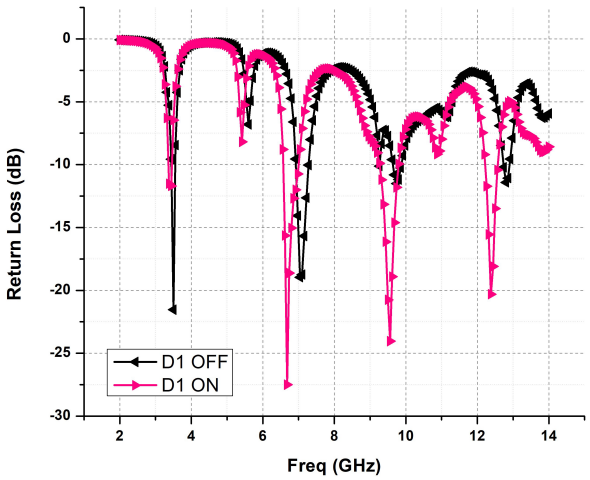

Figure 11. Return loss plot showing the effect of diode D_1 under On and Off switching conditions.

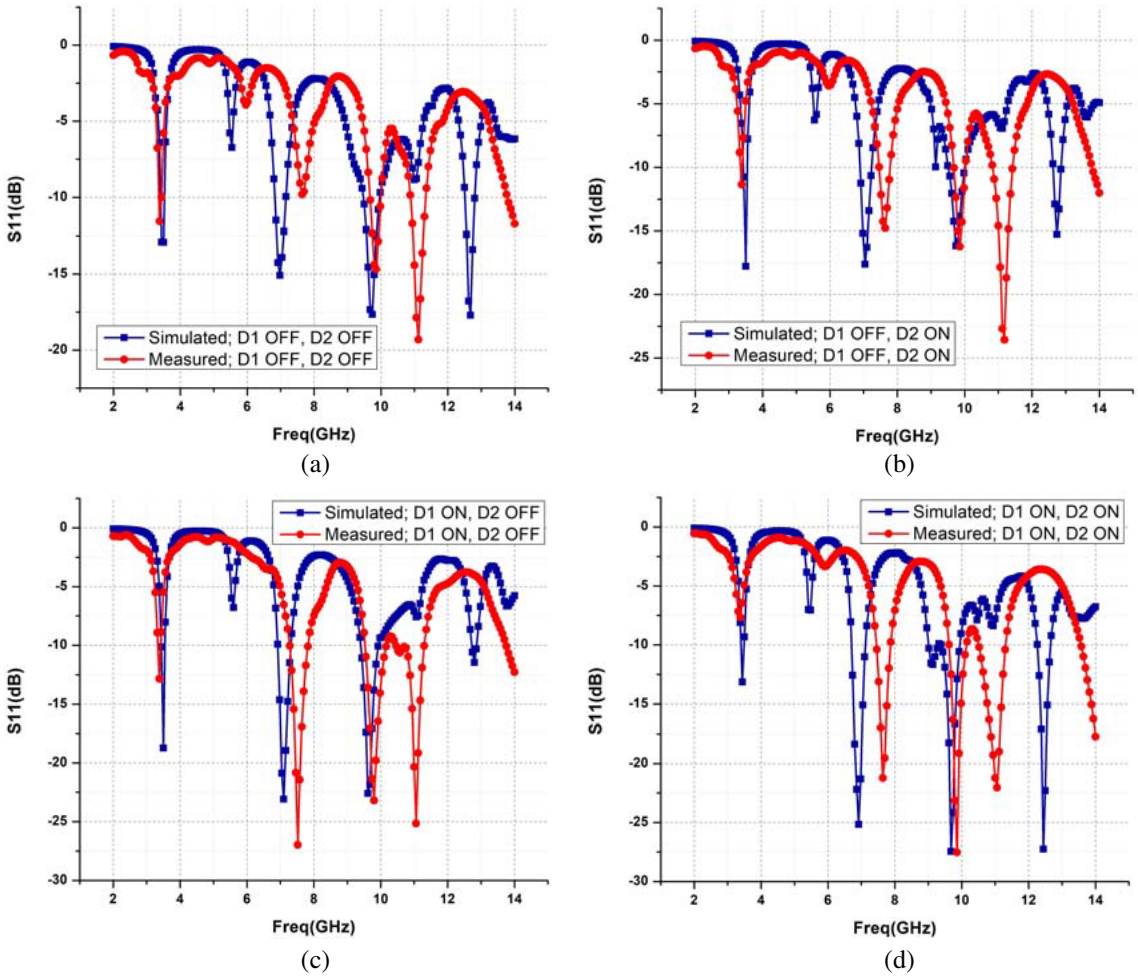

Figure 12. Variation of S_{11} (dB) parameter with frequency of proposed FRA for various diode states (a) D_1 OFF and D_2 OFF, (b) D_1 OFF and D_2 ON, (c) D_1 ON and D_2 OFF, (d) D_1 ON and D_2 ON.

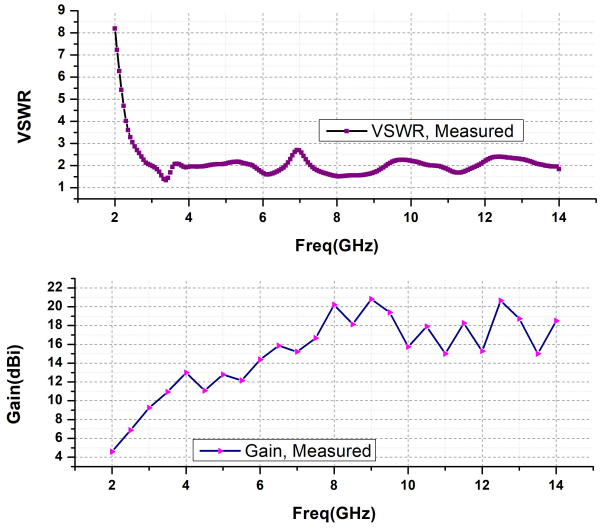

Figure 13. Plot of measured VSWR and measured gain (dBi) as a function of frequency for the proposed FRA.

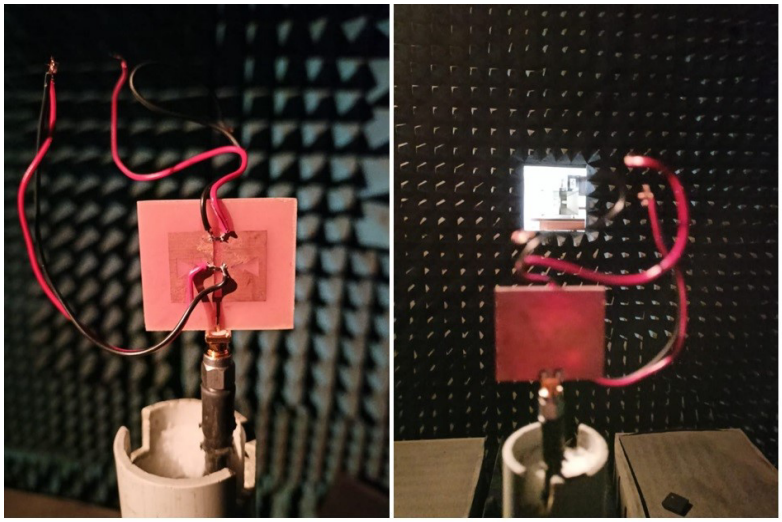

Figure 14. Fabricated prototype in anechoic chamber set-up.

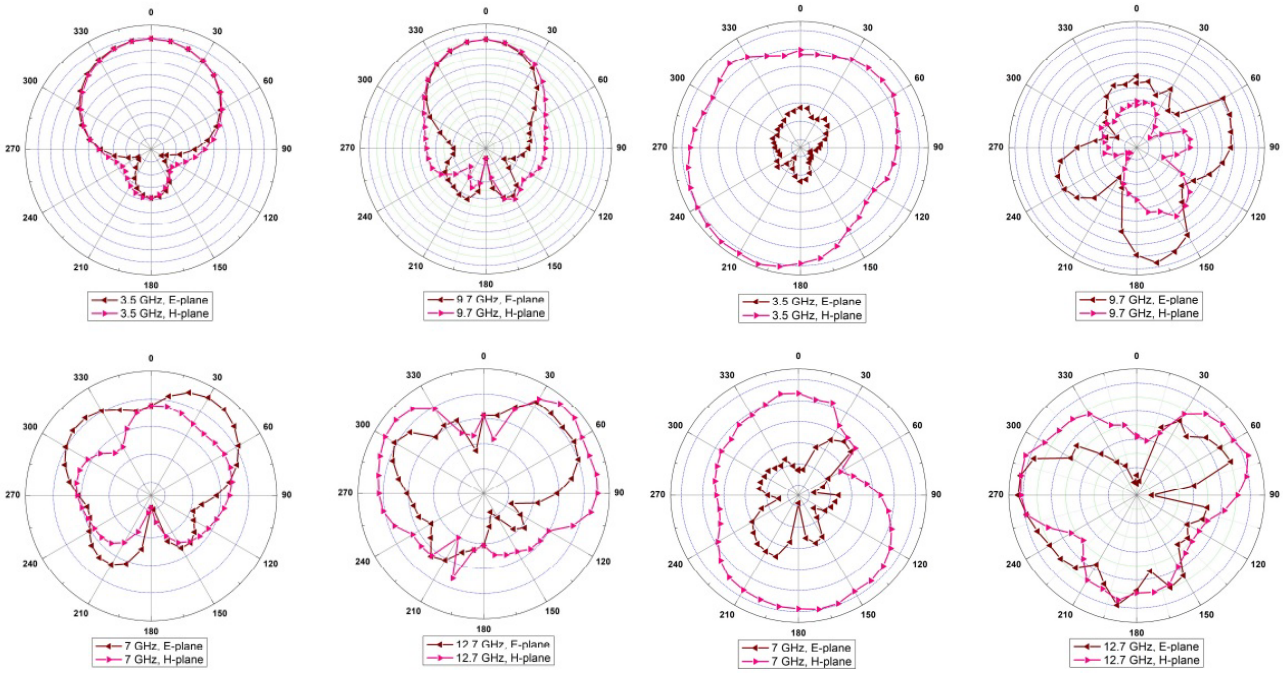

(a) Simulated E and H plane radiation patterns

(b) Measured E and H plane radiation patterns

Figure 15. Simulated and measured far-field radiation patterns of the proposed FRA at 3.5 GHz, 7 GHz, 9.7 GHz and 12.7 GHz.

4. CONCLUSION

Smart communication infrastructures are incomplete without wireless systems that employ antennas capable of electronic reconfiguration. In this dissemination, a multiband Fractal Reconfigurable Antenna (FRA) is presented using two PIN diodes as switching elements to reconfigure the performance parameters of the antenna. The utilization of fractal slots on the radiating patch has reduced the antenna patch area and increased the electrical length yielding lower resonant frequencies and more operating bands. The proposed FRA provides operating bandwidths in the S, C, and X microwave bands with

reconfigurable properties in terms of bandwidth and gain by incorporating only two RF PIN diodes. Besides exhibiting multiband characteristics, the proposed antenna provides electronic reconfiguration of parameters to deliver enhanced performance. It is simple and conformable in structure and is promising for multiband and multifunctional current and future smart wireless applications.

CONFLICT OF INTEREST

The authors declare that they have no known conflict of interest that could have influenced the work presented in this manuscript.

ACKNOWLEDGMENT

The author is extremely grateful to the University Grants Commission (UGC), India for providing financial assistance (NET JRF) to this research work (UGC-Ref. No.: 3770/ (NET-DEC 2018)).

REFERENCES

1. Gianvittorio, J. P. and Y. Rahmat-Samii, "Fractal antennas: A novel antenna miniaturization technique, and applications," *IEEE Antennas and Propagation Magazine*, Vol. 44, No. 1, 20–36, Feb. 2002, doi: 10.1109/74.997888.
2. Werner, D. H. and S. Ganguly, "An overview of fractal antenna engineering research," *IEEE Antennas and Propagation Magazine*, Vol. 45, No. 1, 38–57, Feb. 2003, doi: 10.1109/MAP.2003.1189650.
3. Arif, A., M. Zubair, M. Ali, M. U. Khan, and M. Q. Mehmood, "A compact, low-profile fractal antenna for wearable on-body WBAN applications," *IEEE Antennas and Wireless Propagation Letters*, Vol. 18, No. 5, 981–985, May 2019, doi: 10.1109/LAWP.2019.2906829.
4. Azari, A., "A new super wideband fractal microstrip antenna," *IEEE Transactions on Antennas and Propagation*, Vol. 59, No. 5, 1724–1727, May 2011, doi: 10.1109/TAP.2011.2128294.
5. Lopes, M., M. N. Aik, and A. Dessai, "Design and simulation of frequency reconfigurable microstrip patch antenna for C band and X band applications," *2017 International Conference on Computing, Communication, Control and Automation (ICCUBEA)*, 1–6, 2017, doi: 10.1109/ICCUBEA.2017.8464009.
6. Majid, H. A., M. K. Abdul Rahim, M. R. Hamid, N. A. Murad, and M. F. Ismail, "Frequency-reconfigurable microstrip patch-slot antenna," *IEEE Antennas and Wireless Propagation Letters*, Vol. 12, 218–220, 2013, doi: 10.1109/LAWP.2013.2245293.
7. Yang, S. S., A. A. Kishk, and K. Lee, "Frequency reconfigurable U-slot microstrip patch antenna," *IEEE Antennas and Wireless Propagation Letters*, Vol. 7, 127–129, 2008, doi: 10.1109/LAWP.2008.921330.
8. Altaf, A., J. Jung, Y. Yang, K. Lee, and K. C. Hwang, "Reconfigurable dual-/triple-band circularly polarized dielectric resonator antenna," *IEEE Antennas and Wireless Propagation Letters*, Vol. 19, No. 3, 443–447, Mar. 2020, doi: 10.1109/LAWP.2020.2970171.
9. Khidre, A., K. Lee, F. Yang, and A. Z. Elsherbeni, "Circular polarization reconfigurable wideband e-shaped patch antenna for wireless applications," *IEEE Transactions on Antennas and Propagation*, Vol. 61, No. 2, 960–964, Feb. 2013, doi: 10.1109/TAP.2012.2223436.
10. Qin, P.-Y., A. R. Weily, Y. J. Guo, and C.-H. Liang, "Polarization reconfigurable U-slot patch antenna," *IEEE Transactions on Antennas and Propagation*, Vol. 58, No. 10, 3383–3388, Oct. 2010, doi: 10.1109/TAP.2010.2055808.
11. Saravanan, M. and M. J. S. Rangachar, "Polarization reconfigurable square patch antenna for wireless communications," *AEM*, Vol. 7, No. 4, 103–108, Sep. 2018.
12. Yang, X., B. Wang, W. Wu, and S. Xiao, "Yagi patch antenna with dual-band and pattern reconfigurable characteristics," *IEEE Antennas and Wireless Propagation Letters*, Vol. 6, 168–171, 2007, doi: 10.1109/LAWP.2007.895292.

13. Nguyen-Trong, N., L. Hall, and C. Fumeaux, "A frequency- and pattern-reconfigurable center-shorted microstrip antenna," *IEEE Antennas and Wireless Propagation Letters*, Vol. 15, 1955–1958, 2016, doi: 10.1109/LAWP.2016.2544943.
14. Tirunagari, A., B. Madhav, C. V. Kumar, P. Sruthi, M. Sahithi, and K. V. Manikanta, "Design of a frequency reconfigurable fractal antenna for Internet of Things (IoT) in vehicular communication," *International Journal of Recent Technology and Engineering*, Vol. 7, 1605–1611, Mar. 2019.
15. Kaur, P., A. De, and S. K. Aggarwal, "Design of a novel reconfigurable fractal antenna for multi-band application," *International Journal of Advanced Science and Technology*, Vol. 62, 103–112, 2014.
16. Chaouche, Y. B., F. Bouttout, I. Messaoudene, L. Pichon, M. Belazzoug, and F. Chetouah, "Design of reconfigurable fractal antenna using pin diode switch for wireless applications," *2016 16th Mediterranean Microwave Symposium (MMS)*, 1–4, 2016, doi: 10.1109/MMS.2016.7803852.
17. Chaouche, Y. B., M. Nedil, and I. Messaoudene, "A bandwidth reconfigurable multiband fractal antenna for wireless applications," *2019 IEEE International Symposium on Antennas and Propagation and USNC-URSI Radio Science Meeting*, 917–918, 2019, doi: 10.1109/APUSNCURSINRSM.2019.8889345.
18. Balanis, C. A., *Antenna Theory, Analysis and Design*, John Wiley and Sons, 2005.
19. Garg, R., P. Bhartia, I. Bahl, and A. Ittipiboon, *Microstrip Antenna Design Handbook*, Artech House, Boston, London, 2003.
20. https://www.nxp.com/docs/en/data-sheet/BAP50-03.pdf.
21. Singh, A., M. Aneesh, Kamakshi, and J. A. Ansari, "Analysis of microstrip line fed patch antenna for wireless communications," *Open Engineering*, Vol. 7, No. 1, 279–286, 2017.
22. Singh, A., J. A. Ansari, Kamakshi, M. Aneesh, S. S. Sayeed, and A. Mishra, "Analysis of slots and notches loaded patch antenna for dualband operation," *IMPACT-2013*, 168–171, 2013, doi: 10.1109/MSPCT.2013.6782111.
23. Ansari, J. A., A. Mishra, N. P. Yadav, et al., "Analysis of L-shaped slot loaded circular disk patch antenna for satellite and radio telecommunication," *Wireless Personal Communications*, Vol. 70, 927–943, 2013.
24. Ansari, J. A., A. Mishra, and N. P. Yadav, "Analysis of U-shaped slot loaded circular disk antenna for dualband operation," *International Journal of Electical Engineering and Embedded Systems*, Vol. 3, 73–77, 2011.
25. Ansari, J. A. and R. B. Ram, "Analysis of broad band U-slot microstrip patch antenna," *Microwave and Optical Technology Letters*, Vol. 50, No. 4, 1069–1073, Feb. 2008.
26. Tiwari, D., J. A. Ansari, M. G. Siddiqui, and A. K. Saroj, "Analysis of modified square sierpinski gasket fractal microstrip antenna for wireless communications," *AEU — International Journal of Electronics and Communication*, Vol. 94, 377–385, 2018.
27. Tiwari, D., J. A. Ansari, A. K. Saroj, and M. Kumar, "Analysis of a Miniaturized Hexagonal Sierpinski Gasket fractal microstrip antenna for modern wireless communications," *AEU — International Journal of Electronics and Communication*, Vol. 123, 153288, Aug. 2020.